High quality ultrathin Bi_2Se_3 films on CaF_2 and CaF_2/Si by molecular beam epitaxy with a radio frequency cracker cell

Li Zhang,[1,2] Robert Hammond,[2] Merav Dolev,[1,2] Min Liu,[2,3] Alexander Palevski,[4] and Aharon Kapitulnik[1,2,3]
[1]*Department of Applied Physics, Stanford University, Stanford, California 94305, USA*
[2]*Geballe Laboratory for Advanced Materials, Stanford University, Stanford, California 94305, USA*
[3]*Department of Physics, Stanford University, Stanford, California 94305, USA*
[4]*School of Physics and Astronomy, Tel Aviv University, 69978 Tel Aviv, Israel*

(Received 25 May 2012; accepted 27 September 2012; published online 8 October 2012)

We report a method to fabricate high quality Bi_2Se_3 thin films using molecular beam epitaxy with a radio frequency cracker cell as an atomic selenium source. With Se-to-Bi ratios close to exact stoichiometry, optimal layer-by-layer growth of high quality Bi_2Se_3 thin films with smooth surfaces has been achieved on $CaF_2(111)$ substrates and $Si(111)$ substrates with a thin epitaxial CaF_2 buffer layer (CaF_2/Si). Transport measurements show a characteristic weak-antilocalization magnetoresistance in all the films, with the emergence of a weak-localization contribution in the ultrathin film limit. Quantum oscillations, attributed to the topological surface states have been observed, including in films grown on CaF_2/Si. © *2012 American Institute of Physics*. [http://dx.doi.org/10.1063/1.4758466]

Topological insulators (TI) are a new type of three-dimensional (3D) bulk insulating materials with surface quantum spin Hall effect states protected by time reversal symmetry. In particular, Bi_2Se_3 exhibits a 0.3 eV bulk gap and a surface state Dirac point exposed in the middle of that gap, thus, identified as an ideal material-platform for applications that use its TI nature.[1,2] High quality thin films of Bi_2Se_3, with a Fermi level able to be tuned to a suitable position that is within the bulk band gap and in the surface state band simultaneously, will be key for its applications in spintronics and quantum information device physics.

Though much effort has been devoted to the fabrication of Bi_2Se_3 thin films, primarily using molecular beam epitaxy (MBE) on a variety of substrates,[3–10] success has been limited due to several critical factors in the deposition process. First, selenium is known to evaporate in the form of Se_x ($x \geq 2$) molecules, with low sticking probability and poor chemical reactivity.[11] As a result, Se is typically introduced during growth at a 15:1 or higher ratio to Bi. However, whether it is the high volatility of Se, or a consequence of thermodynamics at $\sim$300°C substrate temperature, the resulting films always suffer from selenium vacancies and thus are n-doped in the bulk,[12,13] leading to substantial contribution from bulk conduction, challenging the very nature of topological insulators in which only the surface state conducts. Therefore, making high quality Bi_2Se_3 and doped Bi_2Se_3 thin films with efficient usage of Se and desired Fermi level still remains one of the key challenges in the field.

In this letter, we report how we grew high quality Bi_2Se_3 thin films, especially ultrathin films, in a MBE system with a radio frequency (RF) cracker cell for atomic Se source. $CaF_2(111)$ substrates were chosen for their better lattice mismatch with Bi_2Se_3 (7%), much smaller than the 13% mismatch between Bi_2Se_3 and the commonly used $Al_2O_3(0001)$ substrate. $CaF_2(111)$ also acts as an excellent dielectric buffer layer for growth of Bi_2Se_3 films on doped-Si substrates, due to its small, 0.6% lattice mismatch with Si(111). Using highly doped Si(111) substrates, we fabricated high quality backgated Bi_2Se_3 devices on Si substrates after an epitaxial CaF_2 buffer layer was first deposited (CaF_2/Si), which we will introduce briefly in the end. We have also grown Bi_2Se_3 films on $Al_2O_3(0001)$, which yielded similar results to those reported by other groups (see, e.g., Refs. 10 and 13). Since the ultrathin Bi_2Se_3 films on CaF_2 and CaF_2/Si had superior qualities, in this paper, we concentrate on those type of films, and where appropriate, we contrast their properties with films on $Al_2O_3(0001)$.

As shown in Fig. 1, a RF cracker cell for solid source materials contains two major parts that are coupled to each other through a rate valve: a regular Knudsen thermal cell (K-cell) and a RF plasma section. An inert gas plasma is first ignited in the plasma section. The K-cell is subsequently heated up to evaporate the source material into the plasma region. The discharged source material, usually polymeric, will be dissociated into reactive atoms in the plasma section, forming a new plasma of the source material, thus enhancing the reaction with other evaporated materials and the growth of the target material. This technique has previously been applied to generate atomic phosphorus[14] and arsenic[15] for doping. We adapted this technique as a composition source for uniform thin film growth. For our experiments, we installed a RF cracker cell manufactured by SVT Associates in our home-built MBE system and argon was used as the supporting gas, and this enabled us to use lower Se-to-Bi rate ratios during growth, ranging from the exact 3:2 to not more than 3:1, without post-growth annealing.

Highly smooth $CaF_2(111)$ substrates (by CrysTec GmbH) were used, with typical atomic force microscopy (AFM) measured RMS-roughness $\lesssim$0.35 nm over a $1 \times 1\ \mu m$ area. Before loaded inside the MBE system, all substrates were cleaned in chloroform, acetone, and methanol sequentially in an ultrasonic cleaner, 15 min each. After transferred into the growth chamber, the substrates were first outgased at 600 °C for 30 min, then kept at 400 °C and exposed to atomic

Downloaded 06 Jan 2013 to 132.66.11.212. Redistribution subject to AIP license or copyright; see http://apl.aip.org/about/rights_and_permissions

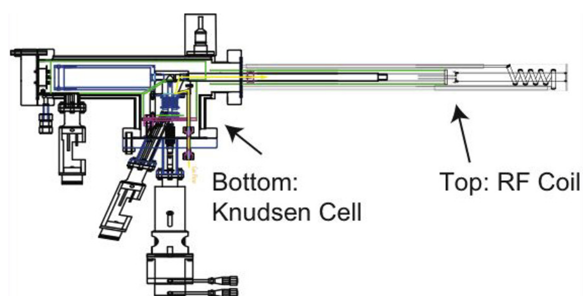

FIG. 1. Diagram of the RF Se cracker used in this study: on the bottom is a Knudsen cell for Se, coupled to a RF coil as the plasma section on the top.

oxygen for 10 min for surface cleaning, with temperature of the substrates monitored in real time by a thermometer attached under the sample holder. No surface reconstructions were observed through reflection high energy electron diffraction (RHEED) monitoring through out this process. High purity Se (99.999%) was evaporated from the RF cracker cell, with the rate controlled by adjusting and maintaining the opening of the rate valve accurately. High purity Bi (99.999%) was evaporated from an electron beam source, controlled by a quartz crystal microbalance (QCM), allowing us to keep both the Bi/Se ratio and the deposition rate constant throughout the growth in a vacuum of 2×10^{-8} Torr where a pure Se plasma (after the Ar gas was turned off) was maintained.

All Bi_2Se_3 films were grown using a two-step procedure.[9] In the first step, the first quintuple layer (QL) of the Bi_2Se_3 film was deposited at 197 °C, then the sample was heated to 226 °C at a 5 °C/min rate, followed by the second step deposition of the film at 226 °C. After the deposition, samples were cooled down immediately without annealing, and pure Se was deposited on some of the samples to prevent fast degradation. The growth procedure described above, using a 1:3 Bi-to-Se ratio and a 0.35 QL/min deposition rate, was found to yield layer-by-layer growth and highest quality ultrathin Bi_2Se_3 films on $CaF_2(111)$ and CaF_2/Si substrates, as will be discussed below.

During the growth, the RHEED patterns of the substrates faded away during the first step. From the beginning of the second step at 226 °C, the peak intensity of the Bi_2Se_3 RHEED pattern would oscillate, indicating layer-by-layer growth. Fig. 2(a) shows that the oscillations observed during the second step growth of a 19 QL thick film, with growth rate about 0.35 QL/min. During the second step growth, the streaky pattern that emerged at the beginning of the second step would become more clear, indicating good crystallinity

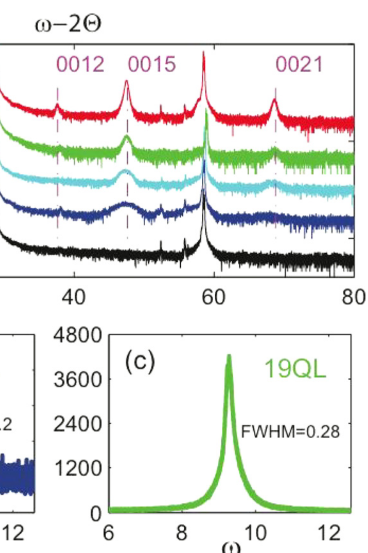

FIG. 3. (a) X-ray diffraction patterns (log scale) for films of different thickness. (b) X-ray rocking curve of the Bi_2Se_3 (006) peak for a 4 QL thick film (linear scale), with FWHM = 0.2°. (c) X-ray rocking curve of the Bi_2Se_3 (006) peak for a 19 QL thick film, with FWHM = 0.28°.

remained throughout the growth. Inset of Fig. 2(a) shows the RHEED pattern captured right after the deposition of the 19 QL film shown in Fig. 2(a).

Topography of the Bi_2Se_3 thin films was examined by AFM using a PARK XE-70 microscope. Fig. 2(b) shows a typical $1\mu m \times 1\mu m$ AFM scan on a 5 QL sample. As seen from the color spread, it is a flat area with some defects and small fluctuations with amplitude smaller than 1 nm. This roughness is attributed to the high vapor pressure of Se, such that after the rate valve of the Se cracker cell was completely closed at the end of deposition, Se vapor in the growth chamber would still remain, until the system cooled down completely.

Crystallinity of the Bi_2Se_3 thin films was studied using x-ray diffraction (XRD). Clear c-axis orientated Bi_2Se_3 peaks were observed in films from 4 QL up to 98 QL thick, as shown in Fig. 3(a). As shown in Figs. 3(b) and 3(c), the FWHM of a 4 QL film and a 19 QL film are 0.2° and 0.28°, respectively, indicating that high crystallinity of Bi_2Se_3 was obtained from the ultrathin limit and well preserved during the layer-by-layer growth.

Transport properties of the Bi_2Se_3 thin films were measured at temperature down to 2 K, with a magnetic field up to 9 T. The measurements were done in a 5 × 5 mm van der Pauw configuration with ohmic Ti/Au contacts. Hall effect

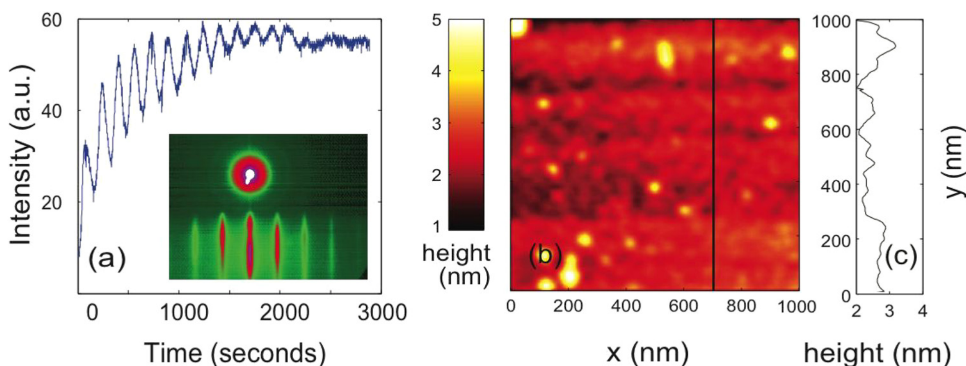

FIG. 2. (a) RHEED oscillations observed during growth of a 19 QL film. Inset is the RHEED pattern of the same 19 QL film captured immediately after deposition. (b) $1\mu m \times 1\mu m$ AFM image taken on a 5 QL thick film. (c) Depth profile of the black line that cut vertically across the sample shows that the fluctuations on top of the sample surface are smaller than 1 nm, and the step size is 1 nm.

Downloaded 06 Jan 2013 to 132.66.11.212. Redistribution subject to AIP license or copyright; see http://apl.aip.org/about/rights_and_permissions

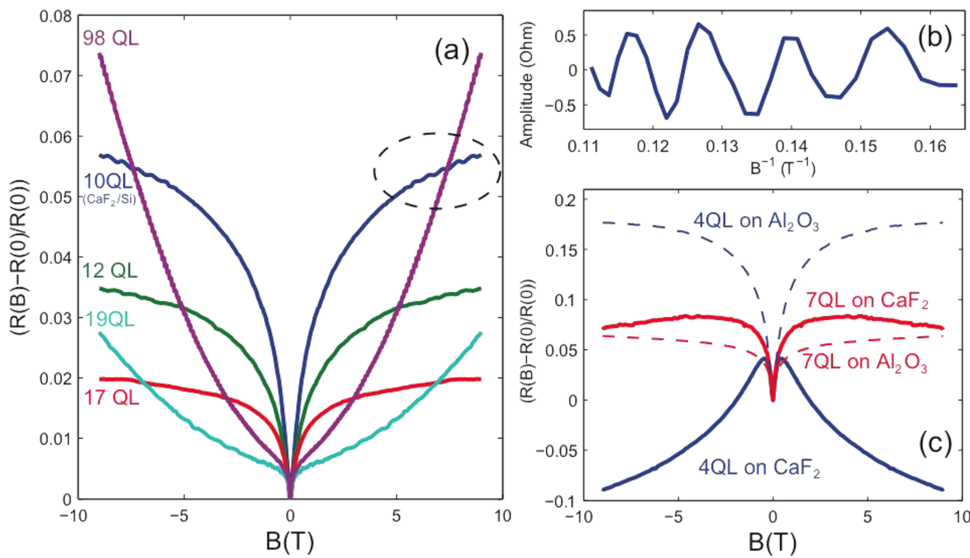

FIG. 4. (a) Magnetoresistance of films of different thickness on CaF_2, among which the 10 QL film was on a $CaF_2/Si(111)$ substrate and the others were on pure CaF_2 substrates. The circle indicates visible quantum oscillations in the 10 QL film, which was plotted in (b) after a smooth background was subtracted. (c) Magnetoresistance of 4 QL and 7 QL films on CaF_2 substrates (solid lines), showing a combination of both WAL and WL effects, compared to 4 QL and 7 QL films on Al_2O_3 (0001) substrates (dashed lines) showing only WAL behavior.

and magnetoresistance (MR) were also measured, from which carrier density and mobility were deduced. At 2 K, all the films investigated, from 4 QL up to 98 QL, showed a strong MR cusp at low perpendicular field [Figs. 4(a) and 4(c)], which can be attributed to the characteristic weak anti-localization (WAL) behavior of the surface states in topological insulators.[16–18] However, in the ultrathin limit, below ~8 QL, a negative MR contribution has been observed on our highest quality films on CaF_2 substrates. Two such examples, a 4 QL film and a 7 QL film, are shown in Fig. 4(c). Negative MR behavior has been reported before,[22,23] for much thicker films (200 and 45 nm/QL) in parallel fields, which was explained as a result of the locking of spin and current direction, and the field was applied in the current direction. Crossover from WAL to weak localization (WL) has also been observed in magnetically doped TI thin films,[24] which was due to the transformation of Bi_2Se_3 from topological insulator to a topologically trivial dilute magnetic semiconductor driven by the magnetic impurities. Fundamentally different from those systems, while the emergence of negative MR (i.e., a WL contribution) in our ultrathin films in perpendicular fields is still not fully understood, it has been proposed via several models that it originates from the bulk bands. For example, quantization of the bulk states at ultrathin limit was predicted to exhibit WL if the Fermi level is close to the bottom of the bulk conduction band, and is crossing a small but finite number of these quantized bands.[19,20] Another possibility is when the thin film is of high quality and the difference between the two opposite topological surfaces is apparent, as to give rise to a gapped Dirac hyperbolas with Rashba-like splittings in energy spectrum due to coupling between opposite topological surfaces.[25,26] More detailed studies of the MR, and the relevance of each of these models to our data will be discussed in a forthcoming publication. For now, it is sufficient to note that any of these explanations require high quality surfaces, at the interface both with the substrate and with vacuum, which is the subject of the present paper.

We also fabricated Bi_2Se_3 thin films on p-doped Si(111) substrates with CaF_2 as buffer layers (CaF_2/Si). The Si(111) substrates were cleaned in buffered oxide etch (BOE) and then loaded inside the MBE immediately. Thin films of CaF_2 were grown epitaxially on Si(111) substrate at 600 °C, with thickness ranging from 12 to 100 nm.[21] After the deposition of CaF_2 and lowering the substrate temperature to 196 °C, growth of Bi_2Se_3 was done following the two-step growth procedure on CaF_2 as described above. We show in Fig. 5 a cross-sectional transmission electron microscopy (TEM) image of a 5 QL Bi_2Se_3 deposited on CaF_2/Si. The 12 nm thick CaF_2 buffer layer grew epitaxially on the Si(111) substrate. And clear quintuple layers of Bi_2Se_3 can be seen, with the thickness of 1 QL about 1 nm. Bi_2Se_3 films on CaF_2/Si were also found to have high crystallinity and characteristic WAL behavior at low temperatures, indistinguishable from films grown on pure CaF_2 substrates. The magnetoresistance of a 10 QL Bi_2Se_3 film on CaF_2/Si was plotted in Fig. 4(a), in which quantum oscillations, measured at 2 K, were clearly visible, especially after a smooth background was subtracted, as shown in Fig. 4(b). From the periods of the oscillations, we obtain a Fermi wave number $k_F = 5.04 \times 10^6$ cm^{-1} and a surface carrier density $n_s = 2.00 \times 10^{12}$ cm^{-2}. Important for our present discussion and relevant for the WL and WAL analysis of TI thin films, on both CaF_2 and CaF_2/Si, is that the pure WAL appears with a much lower scattering rate. Since quantum oscillations are suppressed exponentially for higher scattering rate, we determine that the oscillations indeed come from the surface states. Moreover, Hall effect measured in our films indicates two dimensional carrier density similar to previously measured densities,[3–8,10] while the carrier density

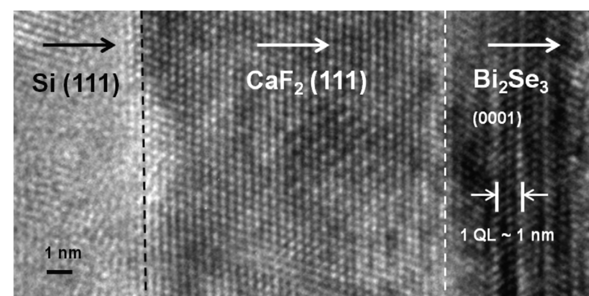

FIG. 5. Cross-sectional TEM image of a 5 QL thick Bi_2Se_3 film grown on Si with a CaF_2 buffer layer about 12 nm thick.

Downloaded 06 Jan 2013 to 132.66.11.212. Redistribution subject to AIP license or copyright; see http://apl.aip.org/about/rights_and_permissions

obtained from the quantum oscillations is one order of magnitude smaller. We also noted that our values of k_F and n_s are very close to the values reported recently for Bi_2Se_3 films on Al_2O_3 substrates of similar thicknesses.[10]

In conclusion, we have demonstrated that a RF cracker cell for Se source can significantly increase the chemical reactivity of evaporated Se by dissociating Se molecules to Se atoms, which enables the deposition of Bi_2Se_3 using a Bi-to-Se ratio close to exact stoichiometry. In high quality ultrathin Bi_2Se_3 films on $CaF_2(111)$ substrates deposited with such a RF cracker cell for atomic Se source, we observed the emergence of weak localization in addition to the commonly observed weak-antilocalization effects, as predicted by theories. After depositing a thin $CaF_2(111)$ layer epitaxially on $Si(111)$ substrate, we were able to grow high quality Bi_2Se_3 films on CaF_2/Si, in which quantum oscillations of the surface states were observed. Those devices can now be gated, paving the way towards the realization of fully functioning back-gated topological insulator devices with tunable Fermi level.

This work was supported by fundings from FENA and DARPA. Merav Dolev and Alexander Palevski were partially funded by a DoE Seed funding for studying TI. We would like to acknowledge Ann Marshall for her help with TEM. We also thank Ko Munakata, Gerwin Hassink, James Analytis, Garrett Hayes, Malcolm Beasley, Jing Wang, Xiaoliang Qi, Shoucheng Zhang, Nicholas Breznay, Nai-Chang Yeh, and Kang Wang for useful discussions.

[1]X. L. Qi and S. C. Zhang, Rev. Mod. Phys. **83**, 1057–1110 (2011).
[2]H. J. Zhang, C. X. Liu, X. L. Qi, X. Dai, Z. Fang, and S. C. Zhang, Nat. Phys. **5**, 438 (2009).
[3]C. L. Song, Y. L. Wang, Y. P. Jiang, Y. Zhang, C. Z. Chang, L. L. Wang, K. He, X. Chen, J. F. Jia, Y. Y. Wang, Z. Fang, X. Dai, X. C. Xie, X. L. Qi, S. C. Zhang, Q. K. Xue, and X. C. Ma, Appl. Phys. Lett. **97**, 143118 (2010).
[4]Y. Zhang, K. He, C. Z. Chang, C. L. Song, L. L. Wang, X. Chen, J. F. Jia, Z. Fang, X. Dai, W. Y. Shan, S. Q. Shen, Q. Niu, X. L. Qi, S. C. Zhang, X. C. Ma, and Q. K. Xue, Nat. Phys. **6**, 584 (2010).
[5]X. Liu, D. J. Smith, J. Fan, Y. H. Zhang, H. Cao, Y. P. Chen, J. Leiner, B. J. Kirby, M. Dobrowolska, and J. K. Furdyna, Appl. Phys. Lett. **99**, 171903 (2011).
[6]L. He, F. Xiu, Y. Wang, A. V. Fedorov, G. Huang, X. Kou, M. Lang, W. P. Beyermann, J. Zou, and K. L. Wang, J. Appl. Phys. **109**, 103702 (2011).
[7]C. Z. Chang, K. He, L. L. Wang, X. C. Ma, M. H. Liu, Z. C. Zhang, X. Chen, and Q. K. Xue, SPIN **1**, 21 (2011).
[8]Y. S. Kim, M. Brahlek, M. Bansal, E. Edrey, G. A. Kapilevich, K. Lida, M. Tanimura, Y. Horibe, S. W. Cheong, and S. Oh, Phys. Rev. B **84**, 073109 (2011).
[9]N. Bansal, Y. S. Kim, E. Edrey, M. Brahlek, Y. Horibe, K. Iida, M. Tanimura, G.-H. Li, T. Feng, H.-D. Lee, T. Gustafsson, E. Andrei, and S. Oh, Thin Solid Films **520**, 224 (2011).
[10]A. A. Taskin, S. Sasaki, K. Segawa, and Y. Ando, Phys. Rev. Lett. **109**, 066803 (2012).
[11]W. C. Cooper and R. A. Westbury, in *Selenium*, edited by R. A. Zingaro and W. C. Cooper (Van Nostrand, New York, 1973), Chap. 3.
[12]J. G. Analytis, J. H. Chu, Y. L. Chen, F. Corredor, R. D. McDonald, Z. X. Shen, and I. R. Fisher, Phys. Rev. B **81**, 205407 (2010).
[13]Z. Alpichshev, R. R. Biswas, A. V. Balatky, J. G. Analytis, J. H. Chu, I. R. Fisher, and A. Kapitulnik, Phys. Rev. Lett. **108**, 206402 (2012).
[14]L. C. Calhoun and R. M. Park, J. Appl. Phys. **85**, 490 (1999).
[15]H. J. Lugauer, A. Waag, L. Worschech, W. Ossau, and G. Landwehr, J. Cryst. Growth **161**, 86–89 (1996).
[16]L. Fu and C. L. Kane, Phys. Rev. B **76**, 045302 (2007).
[17]J. Chen, H. J. Qin, F. Yang, J. Liu, T. Guan, F. M. Qu, G. H. Zhang, J. R. Shi, X. C. Xie, C. L. Yang, K. H. Wu, Y. Q. Li, and L. Lu, Phys. Rev. Lett. **105**, 176602 (2010).
[18]M. Liu, C.-Z. Chang, Z. Zhang, Y. Zhang, W. Ruan, K. He, L.-l. Wang, X. Chen, J.-F. Jia, S.-C. Zhang, Q.-K. Xue, X. Ma, and Y. Wang, Phys. Rev. B **83**, 165440 (2011).
[19]H. Z. Lu and S. Q. Shen, Phys. Rev. B **84**, 125138 (2011).
[20]I. Garate and L. Glazman, Phys. Rev. B **86**, 035422 (2012).
[21]G. C. L. Wong, D. Loretto, E. Rotenberg, M. A. Olmstead, and C. A. Lucas, Phys. Rev. B **48**, 5716 (1993).
[22]J. Wang, H. Li, C.-Z. Chang, K. He, J. S. Lee, X.-C. Ma, N. Samarth, Q.-K. Xue, M. Xie, and M. H. W. Chan, e-print arXiv:1108.1465v1.
[23]H. D. Li, Z. Y. Wang, X. Kan, X. Guo, H. T. He, Z. Wang, J. N. Wang, T. L. Wong, N. Wang, and M. H. Xie, New J. Phys. **12**, 103038 (2010).
[24]M. H. Liu, J. S. Zhang, C. Z. Chang, Z. C. Zhang, X. Feng, K. Li, K. He, L. L. Wang, X. Chen, X. Dai, Z. Fang, Q. K. Xue, X. C. Ma, and Y. Y. Wang, Phys. Rev. Lett **108**, 036805 (2012).
[25]W.-Y. Shan, H.-Z. Lu, and S.-Q. Shen, New J. Phys. **12**, 043048 (2010).
[26]T. V. Menshchikova, S. V. Eremeev, and E. V. Chulkov, JETP Lett. **94**, 106 (2011).

Downloaded 06 Jan 2013 to 132.66.11.212. Redistribution subject to AIP license or copyright; see http://apl.aip.org/about/rights_and_permissions